Screen-space VPL propagation for real-time indirect lighting

Vítor M. Aranha
Departament of Computer Science,
Federal University of Bahia,
Salvador, BA, Brazil
Email: vitormoraesaranha@gmail.com

Márcio C. F. Macedo
Departament of Computer Science,
Federal University of Bahia,
Salvador, BA, Brazil
Email: marciocfmacedo@gmail.com

Antonio L. Apolinario Jr
Departament of Computer Science,
Federal University of Bahia,
Salvador, BA, Brazil
Email: antonio.apolinario@ufba.br

***Abstract*—Reproducing indirect lighting in real time for 3D scenes is a computationally intensive task, but its results add realism and visual fidelity to game-like scenarios and applications. Previous attempts to solve this task explored the use of paraboloid shadow maps for hemispherical visibility queries and Virtual Point Lights (VPLs) for light transport simulations. In our work we aimed at reproducing up to two diffuse bounces of light, while maintaining real-time framerates. We propose an extension to clusterization-based methods in order to sample less VPLs per paraboloid shadow map and capture more bounces of light efficiently. We also propose a projection-aware sampling method to improve sampling efficiency. Our experiments show that, with our approach, it is possible to generate two-bounce VPLs in real time even for low-end commodity GPUs, providing a fast method for indirect illumination.**

I. Introduction

Reproducing the many interactions of light with the ambient yields realistic and pleasing images while providing visual cues about the materials in a scene. Consequently, it is now commonplace for movies, games or architecture applications to employ global illumination techniques in their products in order to enhance their user experiences.

The full light transport phenomenon can be severely demanding to be recreated computationally under strict time constraints such as the ones typically found in the game industry. To solve that problem many techniques were developed such as Path-Tracing [1] and Photon Mapping [2]. The former devises a path-based formulation of the light travelling through a medium, tracing rays to check for visibility between objects. Photon Mapping consists in estimating the distribution of light energy in the form of photons over a scene and finally computing the radiance by gathering the contribution of nearest neighbor photons to obtain the final image. Instant Radiosity [3] is a light transport method that suggests tracing paths from the primary light source through geometry and assigning Virtual Point Lights (VPLs) to its vertices. After rendering the scene from the viewpoints of these VPLs, it is possible to reproduce realistic lighting conditions at interactive rates given that enough VPLs are used. However, this technique requires a high number of rendering passes over geometry, which prevents the algorithm from achieving real-time performance even on the current commodity graphics hardware. Therefore, techniques that speed up the process of solving these visibility queries can be considered essential to algorithms willing to reproduce global illumination effects in real time.

Alternatively, pull-push methods [4] to reconstruct many low resolution shadow maps in parallel using the graphics pipeline have been suggested as well, but while interactive rates can be achieved, geometry preprocessing and thousands of VPLs are necessary to reproduce coherent images, imposing constraints to the algorithm.

A group of algorithms such as the Deep G-Buffer [5] and Directional Occlusion [6], specialize in using only screen-space information to approximate Global Illumination effects in real time, but while they achieve fast framerates, problems such as flickering and excessive viewer-dependence make them unstable and limit their use cases.

Clusterization techniques offer a practical solution to minimize the number of times a scene must be rasterized. By rendering the geometry for a small subset of Virtual Area Lights only, groups of VPLs geometrically similar can reuse shadow tests and speed-up shading of first bounce indirect illumination. Since VPLs are, in general, point light sources, cube mapping is a common approach to render a scene from the point of view of each VPL, but the fact that it requires six passes over geometry, one for each cube face, makes it prohibitive to real-time scenarios with many dynamic elements on screen. A common solution to reduce the cost of that step to one geometry pass per VPL is to use paraboloid maps [7] rather than cube maps. However, despite being faster than cube maps, paraboloid projections may suffer from visual artifacts as we must perform non-linear calculations while the hardware pipeline is bound to linear interpolations. Another possible shortcoming of a paraboloid map is that it projects an ellipse over a rectangular area on screen and typical screen-space sampling methods rely on unit-box samples to choose texels from 2D images.

In this paper we propose Screen-Space VPL Propagation (SSVP), a method based on merging the speed of screen-space algorithms with the stability of world-space approaches to the field of global illumination. By using a pseudo-random sampling method for paraboloid shadow maps that approximates the projection of an elliptical paraboloid in a 2D texture, the probability of samples falling under empty or incoherent areas of the projected image is eliminated, consequently allowing for

plausible real-time propagation of indirect bounces of light in the scene in fast real-time framerates. The 2D paraboloid maps are rendered as Reflective Shadow Maps [8] and propagation is achieved by pseudo-random uniform sampling on these textures to access position, normals and color data.

The main contributions of our technique are the following:

- A fast way to reproduce up to two bounces of diffuse indirect lighting for 3D scenes.
- An efficient method of sampling from paraboloid shadow maps.

II. Related Work

Many algorithms attempt at solving the rendering equation for a diverse set of effects and time constraints. General techniques that focus on realistically representing a broad range of emerging lighting phenomena such as Path Tracing [1] and Photon Mapping [2] are typically used in offline rendering scenarios like movies.

To maximize real-time performance we adhere to VPL techniques, also known by the name of many-light rendering. Several techniques for VPL-based rendering have been proposed in literature. Their popularity rose specially due to being easy to integrate in traditional GPU pipelines with good scalability and performance. In this section, we present a review of the most relevant work related to our approach. For further reading, we suggest the reader to see [9], a comprehensive survey on the historical development of many-light methods.

Reflective Shadow Maps (RSMs) [8] increments shadow maps by storing additional layers with the position, normal and radiant flux of each rendered texel. Shading of each pixel is performed by gathering light contribution from VPLs sampled from the RSM. In this case, hundreds of VPLs are needed to provide plausible images. In order to improve RSM performance, a splatting approach [10] has also been suggested, though it does not attempt to solve visibility, leading to undesired light leaks.

Shading with *Interleaved Sampling* [11] is a common technique used with many-light methods to alleviate the cost of shading a pixel with multiple light sources by splitting a G-Buffer into smaller, lower resolution interleaved buffers. Each buffer computes contribution from a subset of lights only, and, in a further step, the buffers are merged again and a denoising filter is applied to remove undesired artifacts. A buffer translation algorithm was also presented to leverage coalesced memory access in GPUs and maximize performance.

The pull-push based approach of the *Imperfect Shadow Maps* [4] attempts to reconstruct point-based geometry rendered from the points of view of thousands of VPLs into low resolution buffers. Drawing inspiration from *Virtual Spherical Lights* [12], a clustering based approach was developed in [13] reducing the number of visibility calculations. Although real-time performance was achieved, lighting was limited to single-bounce indirect illumination only.

Virtual Gaussian Spherical Lights [14] represent the radiant intensity of VPLs using spherical gaussians. Built on the basis of VPLs generated by an RSM, the spherical gaussian representation can be calculated by mipmapping the shadow map texture on the GPU. In this representation, VPLs are extracted by filtered importance sampling RSMs. For high frequency illumination, such as caustics, a bidirectional RSM is suggested. This approach supports real-time indirect illumination, but the lighting effect may be overblurred due to algorithm bias.

Sequential Monte Carlo Instant Radiosity [15] builds a temporally coherent distribution of VPLs with a heuristic sampling method that preserves certain groups of VPLs between frames. Light paths traced from the primary light source also take in account surfaces that are indirectly visible from the camera, aiming to put VPLs on points that will better influence the final image. The interactive frametimes of this method however makes it unfit for dynamic real-time applications.

Screen-Space approaches such as [6] and [16] aim to reuse rasterized scene data to approximate indirect illumination effects. Tradeoffs between speed of computation and visual quality are often the goal of these techniques. Unfortunately, solving temporal incoherence is a difficult task in this case, due to its high degree of viewer dependence.

With our technique we propose an improvement over the clustered visibility based algorithm [13]. That related work is unable to reproduce more than one indirect light bounce, while our approach calculates up to a second bounce. We use a many-light screen-space approach based on the 2D paraboloid projection of the scene as an RSM. However, instead of sampling from the unit square, points are generated in a shape that minimizes out-of-bound texels, closely packing them together over the projection of the elliptical paraboloid. SSVP is a view-independent fast approximation to indirect lighting that aims at a compromise between speed and quality, while providing temporal coherency.

III. Screen-Space VPL Propagation

Figure 1 shows an overview of SSVP's pipeline. We assume a G-Buffer [17] and an RSM [8] as inputs to our VPL propagation pipeline (Figure 1a). The main idea behind SSVP is to generate VPLs up to a second bounce without resorting to expensive ray tracing. VPLs are created from RSMs (Figure 1b) and clustered to reduce the cost of computing visibility for the entire set of point lights (Figure 1c). We leverage the paraboloid projection of a cluster's visibility in order to sample new surface points and efficiently generate new bounces of light (Figure 1d). In the next subsections we explain the details of each step in SSVP's pipeline.

A. First-Bounce VPL Creation

The scene is rendered from the point of view of the light source and position, normals, albedo and depth are stored in 2D textures (Figure 1a). Shadow map and RSM generation are also decoupled here, this way we can adjust for quality and performance of each step separately. Some approaches suggest the importance sampling of VPLs by their contribution to the

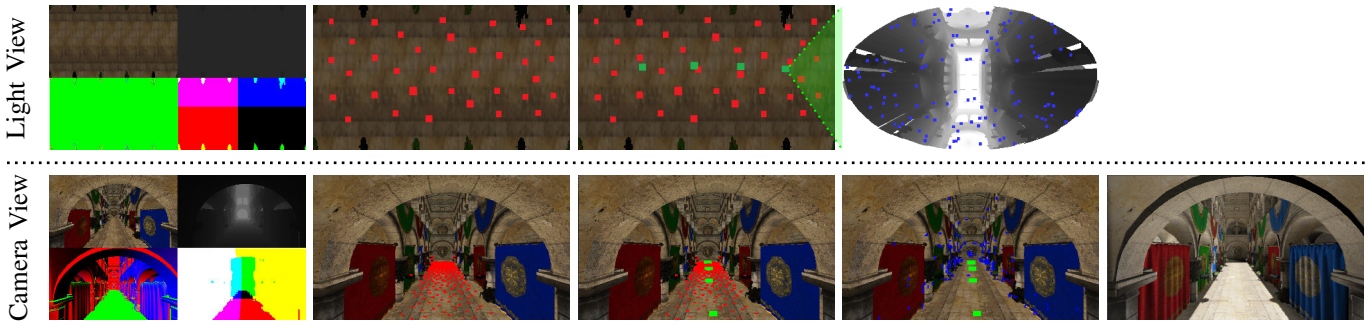

(a) G-Buffer Rendering (b) First-bounce VPL Sampling (c) First-bounce VPL Clustering (d) Second-bounce VPL Sampling (e) Final Rendering

Fig. 1. An overview of our SSVP pipeline. First, the scene is rendered from the camera's viewpoint to a G-buffer. Next, we render from the viewpoint of the main light source to generate our RSM. In both cases we store depth, world-space position, albedo and normals (a). First-bounce VPLs (red squares) are sampled over the scene from the RSM (b). Afterwards, clusters (green squares) are generated by grouping similar VPLs (c). For each cluster, we generate a paraboloid map and perform a unit-disk sampling to distribute second-bounce VPLs (blue squares) over the scene (d). Shading is performed by gathering the contribution of the VPLs in the final stage (e).

scene [4], but while visual quality is favored in such techniques, when used in conjunction with VPL clusters, temporal coherence is harmed by incoherent VPL positions between frames. Therefore standard uniform sampling is employed with a low discrepancy sequence, in this work 256 samples from a 2D Hammersley sequence [18] are used. The set of the first n 2D points of this sequence is defined in Equation 1, where γ is the Van der Corput sequence. Figure 1b illustrates the positioning of the first-bounce VPLs on the scene.

$$\left(\frac{k}{n}, \gamma(k)\right) \text{ for k = 0, 1, 2 ... } n\text{-1} \tag{1}$$

B. VPL Clustering

To reduce the number of visibility queries required to generate the final scene, a traditional K-means algorithm is used to cluster the VPLs. The number of clusters is a user-defined input parameter. At the beginning of the first iteration, a random VPL is chosen as the centroid seed for each cluster. Then, a VPL is assigned to the cluster whose distance between its centroid and the respective VPL is smaller than the distance to other clusters. This process is repeated untill convergence, when the average position and normal of a centroid does not change between iterations. In our tests we identified this value to be a function of the number of clusters used, in our tests no more than 5 iterations were enough to converge.

Because we would also like to mitigate the temporal incoherence between frames, we adopt a strategy of reusing the previous cluster positions for each successive frame. This approach also speeds up the stability and convergence of centroids between K-means iterations.

The traditional way of computing the distance between a VPL and a cluster centroid is to use only the Euclidean distance between them. However, this approach is subject to many artifacts, leading to centroids being completely occluded, inside geometry and leaking light. This happens because VPLs can be positioned closely together but pointing in completely different directions.

To solve this problem, the distance metric must take in account the similarity between normals, allowing the computations to capture geometric information such as coplanarity and main direction, mitigating possible artifacts. For this reason SSVP uses the metric proposed by Dong *et al* [13] as we show in Equation 2.

$$D_{ij} = w_1\|\mathbf{V}_i - \mathbf{C}_j\| + w_2(\mathbf{n}_i \cdot \mathbf{n}_j)^+ \tag{2}$$

D_{ij} is the distance between the i-th VPL to the j-th cluster. $\mathbf{V}_i$ is the position of VPL i and $\mathbf{C}_j$ is the position of a cluster j. $\|\mathbf{V}_i - \mathbf{C}_j\|$ corresponds to the Euclidean distance between a cluster centroid and a VPL. Weighting factors w_1 and w_2 adjust the influence of both the Euclidean distance and the dot product between normals. Favoring one over the other will lead to centroids being positioned inconveniently, inside surfaces or floating in the air. For this reason based on empirical experience we suggest the use of balanced values with similar or close values, here we used $w_1 = 0.6$ and $w_2 = 0.4$. Finally $(\mathbf{n}_i \cdot \mathbf{n}_j)$ is the dot product between the normals of a VPL and a cluster respectively,the notation $+$ means we are clamping the cosine to positive values. All the attributes used in this stage are obtained from our first-bounce VPLs sampled in the previous stage.

C. Second-Bounce VPL Sampling

Once the clusters are generated, the algorithm is ready to solve the visibility computations needed to sample second-bounce VPLs. A hemispherical visiblity map is rendered from the viewpoint of each cluster centroid (Figure 1d) in this stage. The advantage of using paraboloid projections, is that the number of rasterization passes over the geometry are reduced to 1 per cluster. In comparison, hemicube approaches would require 5 rasterization passes per cluster, greatly increasing the cost of sampling. This step is performed with geometry shaders in SSVP's pipeline to leverage the use of layered textures. A resolution of 256^2 pixels is sufficient here.

A naive approach to sample texels from paraboloid maps is to reuse the sampling coordinates from the previous step in the pipeline. However, that scheme does not take in account that the 2D projection of the paraboloid is a filled ellipse and the random values from our previous texture were computed inside the bounds of a unit square.

Rather, we need a method that can generate better samples, arranged inside or very close to the filled ellipse at the center of the 2D texture. To achieve that we analyze the equation of the paraboloid that is used for this projection [7]:

$$f(x, y) = \frac{1}{2} - \frac{1}{2}(x^2 + y^2) \tag{3}$$

An elliptic paraboloid is defined as follows:

$$f(x, y) = \frac{x^2}{a^2} + \frac{y^2}{b^2} \tag{4}$$

with a and b being the curvature constants of the xy-plane. If we rearrange Equation 3:

$$f(x, y) = \frac{1}{2} - \frac{x^2}{2} - \frac{y^2}{2} \tag{5}$$

Equation 5 corresponds to an elliptical paraboloid translated in the Z axis by a factor of $1/2$, assuming $a^2 = b^2 = 2$ in Equation 4. Also, since the terms a and b are equal, so, in fact, this is a special case of the paraboloid: a circular one. In other words, any horizontal cut of this paraboloid defines a circle. For this reason to generate the sampling pattern we resort to a procedural uniform sampling distribution on the unit circle. A mathematical derivation of how to generate uniform samples over the unit circle is provided in [19]. Our reasoning is led by the observation that a typical unit box sampling over the projected area of the paraboloid is wasteful, as many samples may fall over empty regions of the texture. The results of sampling in the unit circle versus the naive approach can be seen in Figure 2, note that the projections appear elliptical due to the stretching that occurs when blitting from a squared (256^2) buffer to the final viewport (16:9 aspect ratio) for illustrative purposes.

Because a bounce of light carries information of the previous surfaces it bounced off, the paraboloid map's position, albedo and normals textures are read to create the list of second-bounce VPLs and complete this sampling stage.

D. Shading the Scene

Once the list of first and second bounce VPLs is complete, the algorithm is ready to shade the scene (Figure 1e). To mitigate the costs of lighting calculations with many light sources we adhere to an interleaved shading approach [11], splitting the framebuffer into smaller, equal-sized tiles with resolution directly proportional to the number of VPLs. Each tile is shaded by a different subset of lights and then interleaved back together. Because each tile represents only a fraction of the total framebuffer resolution, the number of fragments to shade is reduced considerably per light, with a speed up inversely proportional to the number of light sources per tile.

Because we have two lists of sampled lights, one for first-bounces and another for second-bounces, it is necessary to normalize the shading computations by dividing the contribution of each VPL by the probability of it being selected. Because we adhere to a uniform distribution, that probability is constant and equal to $\frac{1}{N}$ where N is total number of VPLs sampled (including first and second bounces). Equation 6 describes how the irradiance L_o at a point $\mathbf{p}$ is calculated:

$$L_o(\mathbf{p}) = \frac{1}{N} \sum_{i=0}^{N} \phi \frac{\cos(\theta)^+ \cos(\sigma)^+}{\|\mathbf{p} - \mathbf{v}_i\|^2} \tag{6}$$

where L_o is the outgoing radiance at a point $\mathbf{p}$, ϕ is a constant that corresponds to the intensity of the VPL. θ is the angle of the surface normal and light direction. σ corresponds to the angle of a VPL's normal and the direction to the surface point. Finally $\|\mathbf{p} - \mathbf{v}_i\|^2$ is the squared distance between the surface point $\mathbf{p}$ and the VPL $\mathbf{v}_i$.

After shading the radiance buffer, the tiles are interleaved back and denoising is carried with an edge-aware gaussian blur. Here albedo information is not applied over the scene yet, as it would risk blurring finer details. Instead, in a final, post-processing stage, we merge the denoised irradiance buffer with the albedo obtained from the Gbuffer and perform gamma correction and tone-mapping over the buffer as defined in Reinhard et al. [20] to adjust the range of irradiance values to the range of the monitor.

IV. Results

In this section we will analyse the SSVP approach in three aspects: performance, visual quality and temporal coherence. Different parameter configurations are presented as we discuss their influence over the behavior of the algorithm. All tests were performed on a desktop with 16 GB of RAM, an Nvidia GTX 1060, 6GB of VRAM and an Intel CPU i7 4790K. No boost configurations were used. The prototype application was developed in C++ using OpenGL 4.6 API and GLSL for shader programming, running over the Windows 10 Operational System.

A. Rendering Performance

To evaluate the performance of SSVP, we must first analyse the computational cost of each stage of the pipeline. To carry these tests a standard configuration was set to a FULL-HD resolution of 1920x1080 pixels, 256 first-bounce VPLs and 256 second-bounce VPLs. We ran all of the experiments on the Crytek Sponza Scene [21], a common model used in the computer graphics literature due to its similarity to other game-like scenes being used in industry.

A frametime analysis provides the relative time slices of each subroutine in a specific frame of the application. This test is commonly used in profiling real-time rendering software to detect performance bottlenecks and opportunities for optimizations. Figure 3 shows a bar chart of the relative time percentages per pipeline stage.

From Figure 3 we can see that Shading is the most time consuming stage for three of the four selected configurations,

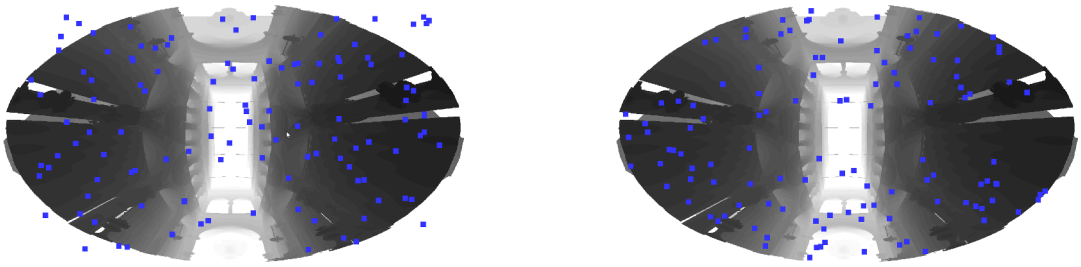

(a) Uniform Unit-Box Sampling (b) Uniform Unit-Disk Sampling

Fig. 2. 120 uniform samples (blue points) in (a) the unit box and (b) the unit disk. In (a), samples are spread over the space without taking the central projection in account. In (b), samples match the projected area in a more coherent pattern.

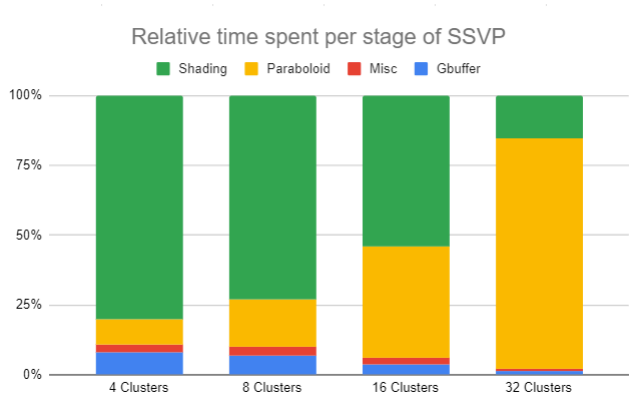

Fig. 3. Average time slices of our algorithm for the Crytek Sponza scene, running on a viewport with 1920x1080 resolution, 4x4 interleaved sampling pattern and multiple cluster configurations. Misc. includes the time to generate a shadow map, to sample first-bounce VPLs with the RSM, to cluster those VPLs, to sample second-bounce VPLs and to denoise the image.

	4 Clusters	8 Clusters	16 Clusters	32 Clusters
Gbuffer	1.03	1.03	1.03	1.03
Misc	0.26	0.29	0.30	0.30
Paraboloid	1.16	2.50	7.90	56.29
Shade	10.31	10.76	10.94	10.95
Denoise	0.13	0.14	0.14	0.18
Total(ms)	12.89	14.74	20.31	68.75

TABLE I
RELATIVE TIME OF EACH SSVP PIPELINE STAGE AS THE NUMBER OF CLUSTERS CHANGE. TIME IS GIVEN IN MILLISECONDS. MISC CORRESPONDS TO THE TIME NEEDED TO GENERATE A SHADOW MAP, TO SAMPLE FIRST-BOUNCE VPLS, TO CLUSTER THOSE VPLS AND TO SAMPLE SECOND-BOUNCE VPLS AND TO DENOISE THE IMAGE.

but the trend decreases as the number of clusters grow. It's relative time slice of SSVP starts at 80% for 4 Clusters and drops to 54% at 16 Clusters. With 32 Clusters, rendering times become dominated by paraboloid rendering and total frametime surpass the real-time threshold by a large amount. Pixel processing operations impose relatively heavy loads over the GPU compared to other tasks, therefore it is expected to be the dominant stage with regard to time per stage of our algorithm.

However, with more and more paraboloid maps requiring computational resources to perform multiple rasterization passes over the geometry, this stage quickly becomes a bottleneck, surpassing shading as the most time consuming step of SSVP. Notice the growth in time as we double the number of paraboloid maps until we reach 16 clusters where a sudden spike makes it grow considerably, then at 32 clusters the total frametime is three times larger than the previous. From this standpoint, analysis of the relative percentual cost reveals that paraboloid creation can quickly become prohibitive for the tight thresholds of real-time rendering. Table I provides the total percentages and rendering times for each configuration. Notice how for configurations of 4 and 8 clusters, the algorithm was able to perform faster than the original 16ms threshold. for real time applications this would be the ideal scenario.

On the other hand, the fastest stages in SSVP's pipeline, K-Means Clustering and VPL sampling account for no more than 0.8% and 0.2% of a single frame for any configuration. The reason behind these low percentages is that clustering here is done on compute shaders to leverage GPU parallelism and sampling is a trivial step that consists of reading texels from paraboloids to create a second-bounce VPL list.

The time curve for different paraboloid configurations grows in a seemingly linear fashion for 4, 8 and 16 Clusters, beyond this point (at the change to 32) time appears to grow with a steeper slope. Preliminary investigation of this behavior implies in increasing cache misses and points synchronization as we grow the number of render passes in geometry shaders, but no experiments with different hardware configurations were performed therefore a decisive evaluation can not be provided here.

B. Visual Quality

To begin the visual quality tests we follow the trend in the computer graphics literature of carrying a ground truth comparison. The ground truth image was generated with the industry standard Path-Tracing technique to render the same Crytek Sponza model using the open source research-oriented renderer Mitsuba [22], with 256 ray samples per pixel. Figure 4 presents a comparison between SSVP and the ground truth. It shows the impact of allowing direct light to bounce two times through the scene, and compare the final image to the ground truth. The addition of second-bounce VPLs introduce

some effects such as color bleeding, seeing nearby the curtains for example and make the shadows brighter, giving a proper sense of indirect lighting.

Ideally we would like to render a visibility map for each VPL in real-time, but as shown in Table I the cost of rendering more paraboloids impact negatively in rendering performance. For this reason, to align with the goals of SSVP, the practical scenario requires a tradeoff between visual quality and performance to favor real-time and game-like applications. To this end, an evaluation of the visual impact of rendering more clusters and more second-bounce VPLs in the final image is carried. We focus on effects that stand out more easily to the human eye, such as color bleeding and artifacts like banding.

Screenshots were taken during navigation of the scene through the same path for 8, 16 and 32 clusters (Figure 5) with 64, 256 and 1024 total second-bounce VPLs. Notice the color bleeding effect nearby the pillars, colored lighting bouncing off the curtains spreads through the floor and the walls, painting them red, blue and green. In these images it is also possible to notice artifacts known as light leaking, due to the lack of precise visibility calculations sometimes light spreads towards unwanted locations, making them brighter than intended. Visually these effects are related mainly to the number of second bounces being rendered, but for larger numbers of clusters more lights are required to achieve a similar levels. Pay attention to Figure 5 how 256 second-bounce VPLs provide clearer colors with 8 clusters in comparison to 16 and 32 clusters respectively. At 1024 VPLs all configurations appear to converge achieving similar results. No further effects arise from higher configurations, but light leaking becomes easier to notice.

A promptly noticeable effect of rendering with reduced cluster count is the amount of banding artifacts on the edges of shadows for single bounce lighting (shadows on the walls and in the back of the scene). As more visibility maps are included, these artifacts tend to soften and for very large numbers of visibility maps (hundreds of thousands [3]) they converge into soft-shadows. However, notice how adding second-bounce VPLs provides a huge benefit in this case, hiding these artifacts by spreading more light over the surfaces and attenuating the banding. This reasoning guides the evaluation in this stage, the fastest possible configuration that still maintains visual plausibility is the one that better fits the objective of SSVP.

Going further in Figure 6 we compare different cluster configurations over the scene using the HDR-VDP-2 metric [23] to evaluate the error between an image and a reference. The scene rendered with the most clusters (32) is used as the baseline and the perceptual error metric is calculated for 16, 8 and 4 clusters.

The root-mean-square error computed for 4 clusters (Figure 6e) is 0.1888, 8 clusters (Figure 6f) is 0.1111 and 16 clusters (Figure 6g) is 0.0936. The higher this value the more likely an observer is to perceive differences in comparison to the reference image. The results from the second-bounce comparison and HDR-VDP-2 imply that 16 clusters offers superior quality over lesser configurations.

C. Temporal Coherence

The temporal coherence of a method evaluates how stable a rendering algorithm performs for animated scenes, with moving cameras or light sources.

To better analyse the coherence of SSVP we point the reader to the videos in the supplemental material. This analysis is complex and deserves a research of its own as can be seen over the literature [24]. However SSVP introduces some techniques to alleviate the impact of flickering when navigating the scene by reusing cluster positions between frames and repeating the sampling patterns. Because of this, SSVP is stable when moving the camera around the scene while keeping the directional light source static. However, with dynamic light sources, a few visual artifacts can be seen as in the black stripe over the red curtain in Figure 7, mainly as a byproduct of cluster visibility changing due to centroids moving along surfaces.

V. Discussion

Starting from the definition that 60 frames per second (16 milliseconds per frame) is the optimal frame rate for hard real-time applications, illumination algorithms must be computed at frame times lower than that threshold, as such applications still need time to compute other tasks such as in-game logic and physics updates. The data in Table I shows that SSVP is able to offer the speed needed for such highly interactive game-like scenarios with average frame rates of 13 milliseconds for the compromise configuration provided. The cost of performing the lighting computations is mitigated here by interleaved sampling, but this stage is expected to become slower as the number of pixels grow, therefore a 1080p FULL-HD resolution is recommended to favor performance. SSVP's visual quality is deeply reliant on the number of clusters we use to compute visibility. However, increasing the number of paraboloid maps too much will beat the purpose of the technique and imply a heavy toll over frame rate. For this reason we would like to render the minimum amount of paraboloid shadow maps that preserves the plausibility of the visuals. The results from the second-bounce comparison and HDR-VDP-2 combined are aligned with our empirical evaluation, leading us to conclude that 8 clusters suffice to preserve visual plausibility with render times within the stabilished threshold of 16 milliseconds.

To enable typically aesthetically pleasing effects such as color bleeding at least 256 second-bounce VPLs are needed for any cluster configuration in the scene tested. Visual perception metrics (HDR-VDP-2) suggest that for the Sponza scene, 8 clusters are enough to plausibly emulate indirect lighting at rates lower than 16 milliseconds. An obvious drawback of our approach is that we are unable to reproduce soft shadows and self-occlusion natively, therefore it is mandatory to resort to orthogonal methods for such effects. Finally, the visual quality of SSVP is directly tied to the number of clusters and second-bounces generated, for this reason increasing first-bounce count will offer no further benefits over quality because of the lack of visibility computations for every new VPL that is introduced. In our experiments 256 first-bounce VPLs proved good enough for our measurements of cluster stability but

(a) SSVP (One Bounce) (b) SSVP (Two Bounces) (c) Path-Tracing (Ground Truth)

Fig. 4. Difference between one (a) and two (b) bounces of light rendered by our technique when compared to the ground-truth (c).

(a) 8 clusters (64 2nd-Bounces) (b) 8 clusters (256 2nd-Bounces) (c) 8 clusters (1024 2nd-Bounces)

(d) 16 clusters (64 2nd-Bounces) (e) 16 clusters (256 2nd-Bounces) (f) 16 clusters (1024 2nd-Bounces)

(g) 32 clusters (64 2nd-Bounces) (h) 32 clusters (256 2nd-Bounces) (i) 32 clusters (1024 2nd-Bounces)

Fig. 5. Sponza rendered from the same viewpoint for different cluster configurations. To compute the number of second bounce VPLs sampled per clusters, divide the total number of VPLs by the number of clusters.

since our method allows for custom parametrization, the reader is encouraged to experiment given custom needs.

VI. Conclusion and Future Works

With SSVP we extended VPL clusterization techniques to reproduce diffuse indirect illumination for up to two diffuse bounces of light under real-time requirements. Given the hard requirements for global illumination in game-like scenarios, we obtained at a method that could represent plausible images under the required time constraints with temporal coherence for moving cameras and reasonable results for dynamic lights. Furthermore, despite mitigating the costs of shading with many light sources, interleaved shading introduces structured noise in the final image. Since removing these prove to be more difficult than typical pseudorandom white-noise, we believe new approaches to shading with many lights could be explored following the research of [25] with monte-carlo methods for VPL selection and distributing noise in a more visually pleasant manner.

Acknowledgment

Márcio C. F. Macedo is financially supported by the Postdoctoral National Program of the Coordination for the Improvement of Higher Education Personnel (PNPD/CAPES), grant number 88882.306277/2018-01. The authors would also like to thank the National Council for Scientific and Technological Development for the financial support.

References

[1] J. T. Kajiya, "The rendering equation," in *Proceedings of SIGGRAPH*. ACM, 1986, pp. 143–150.

[2] H. W. Jensen, "Global illumination using photon maps," in *Rendering Techniques' 96*. Springer, 1996, pp. 21–30.

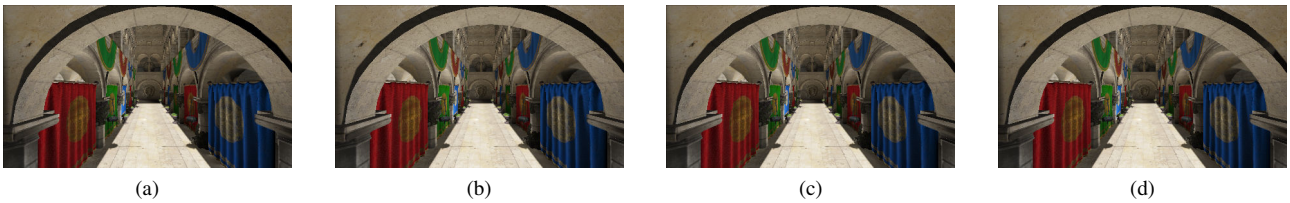

(a) (b) (c) (d)

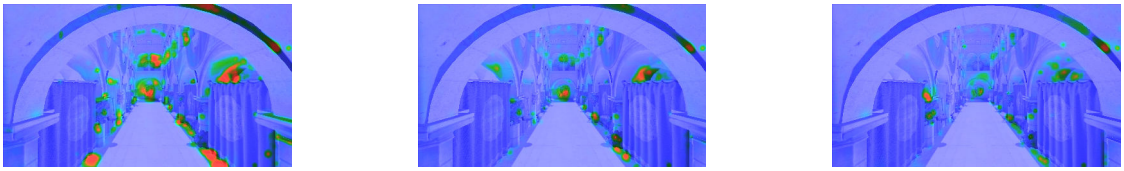

(e) (f) (g)

Fig. 6. HDR-VDP-2 metric applied to images generated with 4, 8 and 16 clusters (Figures 6a, 6b and 6c respectively) in comparison to 32 clusters in Figure 6d. Figures 6e, 6f and 6g show the perceptual error metric for 4, 8 and 16 clusters when compared to the base image with 32 clusters.

(a) (b)

Fig. 7. The visibility map of a moving centroid changes with time with dynamic light sources, potentially causing temporally incoherent visual artifacts as can be seen on the red curtain and the light blotch nearby the blue curtain on the right.

[3] A. Keller, "Instant Radiosity," in *Proceedings of the SIGGRAPH*. ACM, 1997, pp. 49–56.

[4] T. Ritschel, T. Grosch, M. H. Kim, H.-P. Seidel, C. Dachsbacher, and J. Kautz, "Imperfect shadow maps for efficient computation of indirect illumination," in *ACM Transactions on Graphics (TOG)*, vol. 27, no. 5. ACM, 2008, p. 129.

[5] M. McGuire and M. Mara, "Efficient gpu screen-space ray tracing," *Journal of Computer Graphics Techniques (JCGT)*, vol. 3, no. 4, pp. 73–85, 2014.

[6] T. Ritschel, T. Grosch, and H.-P. Seidel, "Approximating dynamic global illumination in image space," in *Proceedings of the I3D*. ACM, 2009, pp. 75–82.

[7] W. Heidrich and H.-P. Seidel, "View-independent Environment Maps." in *Workshop on Graphics Hardware*, 1998, pp. 39–45.

[8] C. Dachsbacher and M. Stamminger, "Reflective shadow maps," in *Proceedings of the I3D*. ACM, 2005, pp. 203–231.

[9] C. Dachsbacher, J. Křivánek, M. Hašan, A. Arbree, B. Walter, and J. Novák, "Scalable realistic rendering with many-light methods," in *Computer Graphics Forum*, vol. 33, no. 1. Wiley Online Library, 2014, pp. 88–104.

[10] C. Dachsbacher and M. Stamminger, "Splatting indirect illumination," in *Proceedings of the I3D*. ACM, 2006, pp. 93–100.

[11] B. Segovia, J. C. Iehl, R. Mitanchey, and B. Péroche, "Non-interleaved deferred shading of interleaved sample patterns," in *Graphics Hardware*, 2006, pp. 53–60.

[12] M. Hašan, J. Křivánek, B. Walter, and K. Bala, "Virtual spherical lights for many-light rendering of glossy scenes," in *ACM Transactions on graphics (TOG)*, vol. 28, no. 5. ACM, 2009, p. 143.

[13] Z. Dong, T. Grosch, T. Ritschel, J. Kautz, and H.-P. Seidel, "Real-time Indirect Illumination with Clustered Visibility," in *Proceedings of the VMV*, vol. 9, 2009, pp. 187–196.

[14] Y. Tokuyoshi, "Virtual Spherical Gaussian Lights for Real-time Glossy Indirect Illumination," in *Computer Graphics Forum*, vol. 34, no. 7. Wiley Online Library, 2015, pp. 89–98.

[15] P. Hedman, T. Karras, and J. Lehtinen, "Sequential monte carlo instant radiosity," in *Proceedings of the I3D*. ACM, 2016, pp. 121–128.

[16] M. Mara, M. McGuire, D. Nowrouzezahrai, and D. P. Luebke, "Deep g-buffers for stable global illumination approximation." in *High Performance Graphics*, 2016, pp. 87–98.

[17] M. Deering, S. Winner, B. Schediwy, C. Duffy, and N. Hunt, "The triangle processor and normal vector shader: a vlsi system for high performance graphics," in *Proceedings of the SIGGRAPH*, vol. 22, no. 4. ACM, 1988, pp. 21–30.

[18] T.-T. Wong, W.-S. Luk, and P.-A. Heng, "Sampling with hammersley and halton points," *Journal of graphics tools*, vol. 2, no. 2, pp. 9–24, 1997.

[19] M. Pharr, W. Jakob, and G. Humphreys, *Physically based rendering: From theory to implementation*. Morgan Kaufmann, 2016.

[20] E. Reinhard, M. Stark, P. Shirley, and J. Ferwerda, "Photographic tone reproduction for digital images," in *Proceedings of the 29th annual conference on Computer graphics and interactive techniques*, 2002, pp. 267–276.

[21] M. McGuire, "Computer Graphics Archive," July 2017. [Online]. Available: https://casual-effects.com/data

[22] W. Jakob, "Mitsuba renderer," 2010, http://www.mitsuba-renderer.org.

[23] R. Mantiuk, K. J. Kim, A. G. Rempel, and W. Heidrich, "Hdr-vdp-2: A calibrated visual metric for visibility and quality predictions in all luminance conditions," *ACM Transactions on graphics (TOG)*, vol. 30, no. 4, pp. 1–14, 2011.

[24] D. Scherzer, L. Yang, O. Mattausch, D. Nehab, P. V. Sander, M. Wimmer, and E. Eisemann, "Temporal coherence methods in real-time rendering," in *Computer Graphics Forum*, vol. 31, no. 8. Wiley Online Library, 2012, pp. 2378–2408.

[25] E. Heitz and L. Belcour, "Distributing monte carlo errors as a blue noise in screen space by permuting pixel seeds between frames," in *Computer Graphics Forum*, vol. 38, no. 4. Wiley Online Library, 2019, pp. 149–158.